Available online at www.sciencedirect.com

ScienceDirect

Ceramics International 42 (2016) 7524–7532

CERAMICS INTERNATIONAL

www.elsevier.com/locate/ceramint

Relationship of microstructure, mechanical properties and titanium cutting performance of TiAlN/TiAlSiN composite coated tool

Xudong Sui, Guojian Li*, Xuesi Qin, Haidong Yu, Xiangkui Zhou, Kai Wang, Qiang Wang

Key Laboratory of Electromagnetic Processing of Materials, Northeastern University, Shenyang 110819, PR China

Received 7 October 2015; received in revised form 23 January 2016; accepted 24 January 2016
Available online 29 January 2016

Abstract

Research on the relationship of microstructure and properties of coated tools such as TiAlN and TiAlSiN plays a key role in obtaining the needed cutting performance in titanium machining. In this study, three kinds of coatings of TiAlN, TiAlSiN monolayer and TiAlN/TiAlSiN composite multilayer have been fabricated by magnetron sputtering method. It is found that the coating structure changes from columnar growth to nanocrystal growth by doping Si element. The TiAlN/TiAlSiN coating is composed by a coarse columnar TiAlN bottom layer and a fine nanocrystalline TiAlSiN top layer. Premature spalling problem (Lc2) is improved by forming the TiAlN/TiAlSiN multilayer structure. Titanium cutting experiment shows that the major wear mechanism of these coated tools is adhesive wear and chipping. The TiAlSiN coated tool has the longest cutting distance at various cutting speeds in these three kinds of coatings. This is because less built-up edge and chipping are generated at the cutting edge due to the dense nanocrystal structure, high hardness and good oxidation resistance of TiAlSiN coating. Therefore, the TiAlSiN coating with dense structure, high hardness and good oxidation resistance is recommended to use in high speed turning titanium.

Keywords: B. Nanocomposites; Coated carbide tool; Titanium cutting; Wear mechanism

1. Introduction

Recently high-strength lightweight titanium alloy structural materials have been widely used with the development of aerospace industry. However, titanium is hard to machine due to its low thermal conductivity, high chemical affinity, and low elastic modulus [1–4]. These characteristics lead to high cutting temperature, short life, and high vibration of cutting tools. Coating on tools has provided an effective way to overcome these problems. Nowadays, a variety of coatings such as TiAlN and TiAlSiN have been proposed in titanium machining [2,5–8]. However, TiAlN coatings prepared by magnetron sputtering generally grow in a columnar mode, which is easy to introduce the crack and to decrease the temperature of oxidation resistance [9,10]. TiAlN coatings doped with Si element have been reported by many researchers to eliminate the columnar crystal and to increase the hardness and oxidation resistance [11,12]. But the adhesion of TiAlSiN was decreased due to the high hardness of the coating [13,14]. It is expected to find a composite way to enhance the cutting performance by improving the adhesion and eliminating the columnar structure simultaneously. Thus, a kind of TiAlN/TiAlSiN multilayer composite coating has been prepared by magnetron sputtering in this study. TiAlN and TiAlSiN monolayer coatings were also prepared in order to compare with the composite coating. Furthermore, all these coatings have been deposited on uncoated carbide turning inserts to conduct the titanium cutting experiments. The titanium cutting performance of these coated tools under various cutting process parameters has been evaluated [15–17]. The relationship of microstructure, mechanical properties and titanium cutting performance of these coatings has been explored.

2. Experiment details

2.1. Coating preparation

All coatings have been prepared on the cemented carbide substrates using a reactive magnetron sputtering method on a

*Corresponding author. Tel.: +86 24 83685649.
E-mail address: gjli@epm.neu.edu.cn (G. Li).

http://dx.doi.org/10.1016/j.ceramint.2016.01.159
0272-8842/

Table 1
Deposition parameters.

Coating	Target power (W)			Deposition time (min)		
	Ti (DC)	TiAl (DC)	Si (RF)	Ti	TiAl	Si
TiAlN	1000	900	–	8	60	–
TiAlSiN	1000	900	200	8	60	60
TiAlN/TiAlSiN	1000	900	200	8	40/20	0/20

multifunctional coating machine. The deposition temperature is 400 °C. The base pressure is $\leq 3 \times 10^{-3}$ Pa. The work pressure is maintained at 0.5 Pa with an argon pressure of 0.35 Pa and a nitrogen pressure of 0.15 Pa. The deposition parameters for each coating are listed in Table 1. Pure Si target (99.99%) and TiAl alloy target (titanium and aluminium atomic ratio is 1:1) were used to deposit the TiAlSiN coating. The targets were cleaned by sputtering in argon gas for 5 min before depositing the coatings. The cemented carbide substrates (YG8, Co: 8 wt%) were polished in turn with diamond abrasive discs and diamond pastes of 2.5 μm until surface roughness (Sq) is lower than 20 nm. Then, substrates were cleaned for 15 min in turn with acetone and ethanol in an ultrasonic cleaner. In this study, titanium buffer layer of about 300 nm thick was deposited preferentially to increase the adhesion force between substrate and coating.

2.2. Cutting experiments

Above three coatings were also deposited on the uncoated cemented carbide turning inserts (YG8, CNMG120408). The Ti–6Al–4V (TC4) bar used in the turning experiments is a typical alpha–beta alloy. Their chemical compositions and mechanical properties are shown in Tables 2 and 3 respectively. A CNC lathe (INTEGREX 200Y, MAZAK®) was used for turning titanium with coolant. The spindle power and maximum speed of the machine are respectively 22.35 kW and 10000 r/min. The cutting depth Vp is 0.5 mm and the feed rate fa is 0.2 mm/r. A general cutting speed of 65 m/min and a higher cutting speed of 100 m/min are selected in this study.

2.3. Characterization of coatings

The morphology and thickness of the coatings were observed by a scanning electron microscope (SEM, SUPRA 35). The attached energy dispersive spectrometer (EDS, OXFORD) was used to evaluate the chemical composition. Structural investigations were tested by a glazing incidence X-ray diffraction (GIXRD, D/MAX 2400) with diffraction angles between 30° and 70° and an incident angle of 1°. Transmission electron microscopy (TEM, Tecnai G2 F30) was used to examine the microstructure. The chemical state of TiAlSiN coatings was determined by an X-ray photoelectron spectroscopy (XPS, ESCALAB250). The hardness was determined by a nanoindenter (Agilent G200) with the indentation depth of about 150 nm and poisson ratio of 0.23. The adhesion strength was tested with a scratch tester (MFT-4000) at a loading rate of 100 N/min and a scratch length of 5 mm.

Table 2
Chemical compositions of TC4 titanium alloy (wt%).

Ti	Al	V	C	N	O	Fe	H
Balanced	5.8–6.7	3.8–4.2	0.15	0.045	0.02	0.33	0.01

3. Results and discussion

3.1. Structure characterization

The compositions of TiAlN and TiAlSiN coatings determined by EDS are respectively $Ti_{0.42}Al_{0.58}N$ and $Ti_{0.39}Al_{0.49}Si_{0.12}N$. The surface morphologies of the coatings are shown in Fig. 1. The TiAlN coating shows a lamellar and loose surface morphology. However, the surface morphology becomes spherical and dense after the introduction of Si element. The TiAlN/TiAlSiN composite coating also exhibits a spherical morphology. The sphere size of composite coating is much smaller than that of the TiAlSiN coating. This may be due to the influence of the TiAlN bottom layer.

The fracture section morphologies of these coatings are also observed by SEM, as shown in Fig. 2. It can be seen that the thickness of these coating is between 1.8 and 2.0 μm. And a titanium buffer layer was also observed. The TiAlN coating has obvious columnar structure characteristic. This leads to the lamellar and loose surface morphology of the TiAlN coating. When Si element is added into the TiAlN coating, the columnar characteristic disappears as shown in Fig. 2(b). In addition, it is also found that the structure of the TiAlN/TiAlSiN composite coating is composed of a columnar structure (about 1100 nm thick, similar to the TiAlN coating) and a fine nanocrystalline structure (about 400 nm thick, similar to the TiAlSiN coating).

XRD and TEM tests were carried out to further explore the coating microstructure. The XRD results reveal that the TiAlN coating has three peaks with the crystal plane index of (111), (200) and (220) as shown in Fig. 3. The peaks of cemented carbide substrate and Ti buffer layer are also detected. It is also found that the width of the diffraction peak broadens and the peak intensity reduces by doping with Si element. The diffraction peak broadens and the peak intensity also reduces. The peak broadening generally means the reduction of grain size or the presence of microstrain [12,14]. Additionally, the selected area electron diffraction (SAED) was also used to confirm the XRD result. The obtained electron diffraction rings are shown in Fig. 2(i) and (ii). An hcp-AlN (102) diffraction ring is found in the TiAlSiN coating and the other rings can be ascribed to cubic fcc TiAlN structure. But no diffraction rings corresponding to the hexagonal structure are detected in the TiAlN coating. Thus, it can be proved that the TiAlSiN coating is mixed cubic and hexagonal structure.

In addition, there is an amorphous peak appearing near 33°, which may be correspond to Si_3N_4 amorphous phase. A similar amorphous peak appears in the composite coating except for the diffraction peaks of the TiAlN coating. In order to ensure the existence of amorphous phase, XPS has been conducted to analyse the TiAlSiN coating. The results are shown in Fig. 4. It can be seen that two peaks at 396.0 eV and 398.9 eV appeared in the N 1 s spectrum. The peak at 396.0 eV is derived from AlN or TiN. The

Table 3
Mechanical properties of TC4 titanium alloy.

Density(kg m^{-3})	Hardness(HRC)	Elastic modulus (GPa)	Yield strength (MPa)	Tensile strength (MPa)	Thermal conductivity W $(m\ k)^{-1}$	Elongation%
4430	36	114	834	935	6.7	14

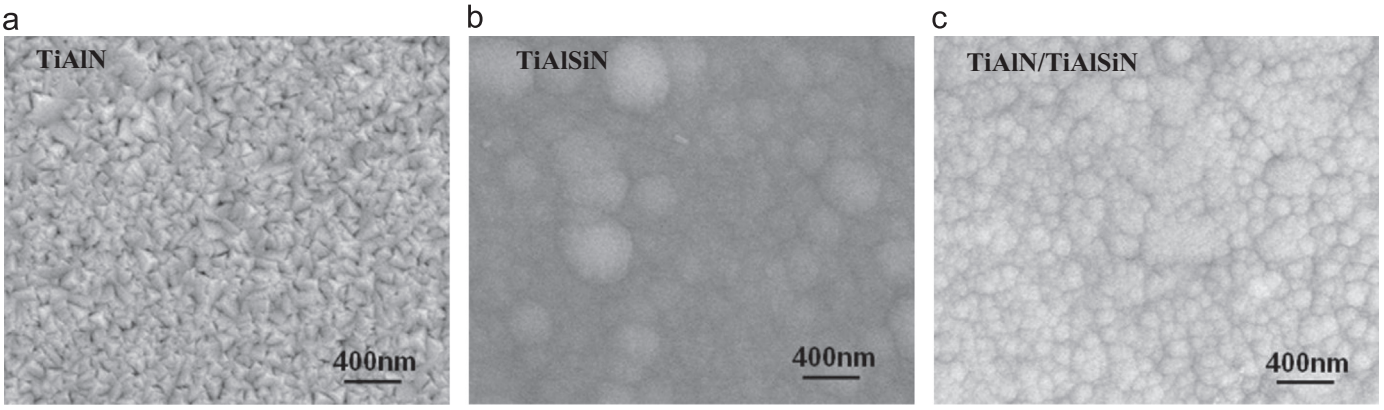

Fig. 1 SEM images of the surface morphologies of different coatings: (a) TiAlN; (b) TiAlSiN; (c) TiAlN/TiAlSiN.

peak at 398.9 eV is derived from Si_3N_4 [12]. Meanwhile, a peak of Si_3N_4 appears at 101.6 eV in the Si 2p spectrum [13]. Above results indicate that Si_3N_4 phase exists in the TiAlSiN coating. However, no obvious diffraction peaks of Si_3N_4 are detected in XRD patterns as shown in Fig. 3. This may be because the Si_3N_4 phase is in amorphous form. Moreover, the selected area electron diffraction results in Fig. 3 show that the ring of the TiAlSiN coating has halo while that of TiAlN coating has no halo. The diffraction halo is derived from the amorphous phase. Thus, it is reasonable to conclude that the Si_3N_4 phase in the TiAlSiN coating.

Fig. 5 gives the bright field TEM images of TiAlN and TiAlSiN coatings. Clearly, the grain size of the TiAlSiN coating is much smaller than that of TiAlN coating. This is the main reason of the XRD peak broadening observed in TiAlSiN diffraction pattern. The decrease of peak intensity of the TiAlSiN coating may associate with a reduced grain size or low degree of crystallinity. In addition, the grain shape also changed from polygon to sphere, which results in the difference surface morphology between TiAlN and TiAlSiN coatings. This can also be observed from the HRTEM images of TiAlSiN coating in Fig. 5(c). According to reference [11], the Si_3N_4 amorphous phase is most likely to be present at the grain boundaries as shown by dashed line in Fig. 5(c). The amorphous phase can strongly suppress the grain coalescence [8,14,18,19] and thus lead to a structure change from columnar to nanocrystalline. This results in different fracture morphologies of TiAlN and TiAlSiN coatings. To summarize, the TiAlN coating has a columnar structure and the TiAlSiN coating was composed by the nanocrystalline embedded in the amorphous matrix. And the TiAlN/TiAlSiN coating is composited by above structures.

3.2. Mechanical properties

The hardness of all the coatings is present in Fig. 6. The hardness of the TiAlSiN coating (22.0 GPa) is higher than that of the TiAlN coating (16.7 GPa) mainly due to its nanocrystalline strucuture. The small grain size of TiAlSiN coating can increase its hardness according to the Hall–Petch formula. In addition, the amorphous phase strengthens the grain boundary and inhibits the extension of dislocation. The hardness of the TiAlN/TiAlSiN composite coating is 20.8 GPa which is higher than that of TiAlN coating but is 5.6% lower than that of the TiAlSiN coating. This may be due to the mixture of columnar and nanocrystal structures. It is noted that the hardness in this paper is relatively lower than the reported value in references [10,11]. This is due to the low density of the coating prepared by magnetron sputtering. The energy of particles in a sputtering method is generally lower than that in an ion plating method. Meanwhile, the hexagonal structure mixed in the TiAlSiN coating may be another reason for the low hardness.

The adhesion strength between coating and substrate was tested by scratch tester, as shown in Fig. 7. The TiAlN coating has the best adhesion strength with the Lc3 value of about 90 N. The adhesion strength of TiAlN/TiAlSiN composite coating is close to the value of TiAlN coating. The good adhesion strength of the TiAlN and TiAlN/TiAlSiN composite coatings may due to their relatively low hardness and columnar structure. Since the structure of Ti interlayer is also columnar as shown in Fig. 2, the stress between TiAlN and Ti is small. This leads to the good adhesion strength. In addition, the TiAlSiN coating spalling occurs earlier at the edge of scratch tracks as shown in Fig. 8(b). This means that the TiAlSiN coating has a lower Lc2 value. It can be observed that the TiAlN/TiAlSiN composite coating improves the premature spalling problem in the TiAlSiN coating by adding a TiAlN bottom layer as shown in the yellow dotted frame in Fig. 8(c). The premature spalling in the TiAlSiN coating may be due to its high hardness and nanocrystal structure [13,14]. The crystal lattice distortion and the existence of amorphous phase around grain boundary will deteriorate the adhesion strength.

Since the crack behaviour and fracture toughness of coatings is very important to the cutting performance in titanium machining [1,20]. A Vickers hardness tester has been used

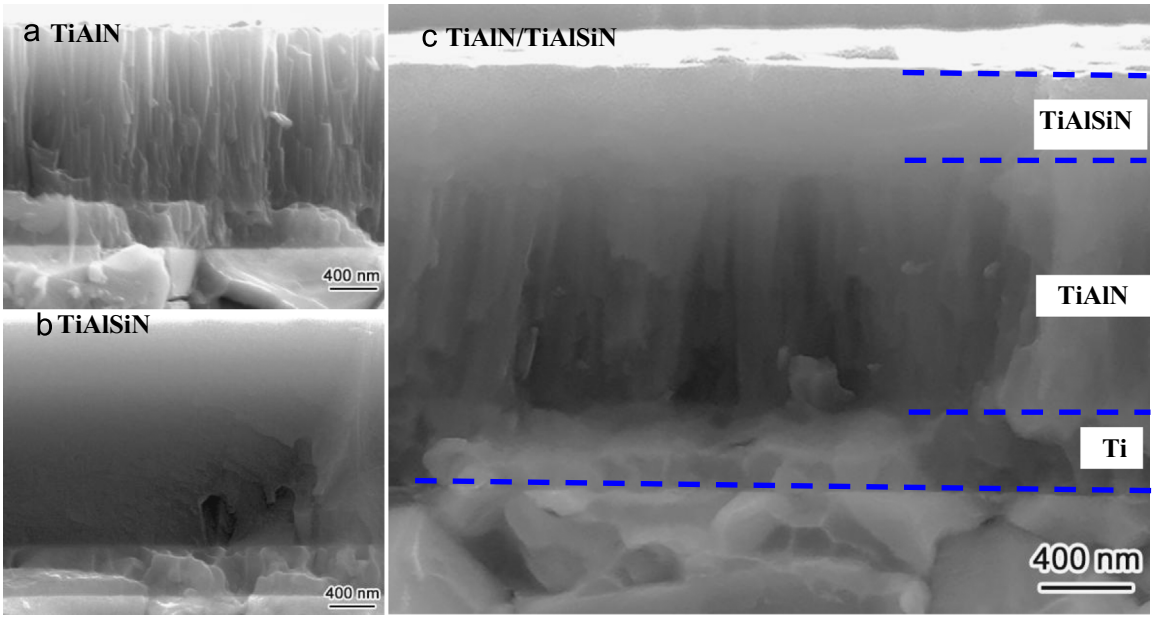

Fig. 2. SEM photos of the fracture section morphologies of different coatings: (a) TiAlN; (b) TiAlSiN; and (c) TiAlN/TiAlSiN.

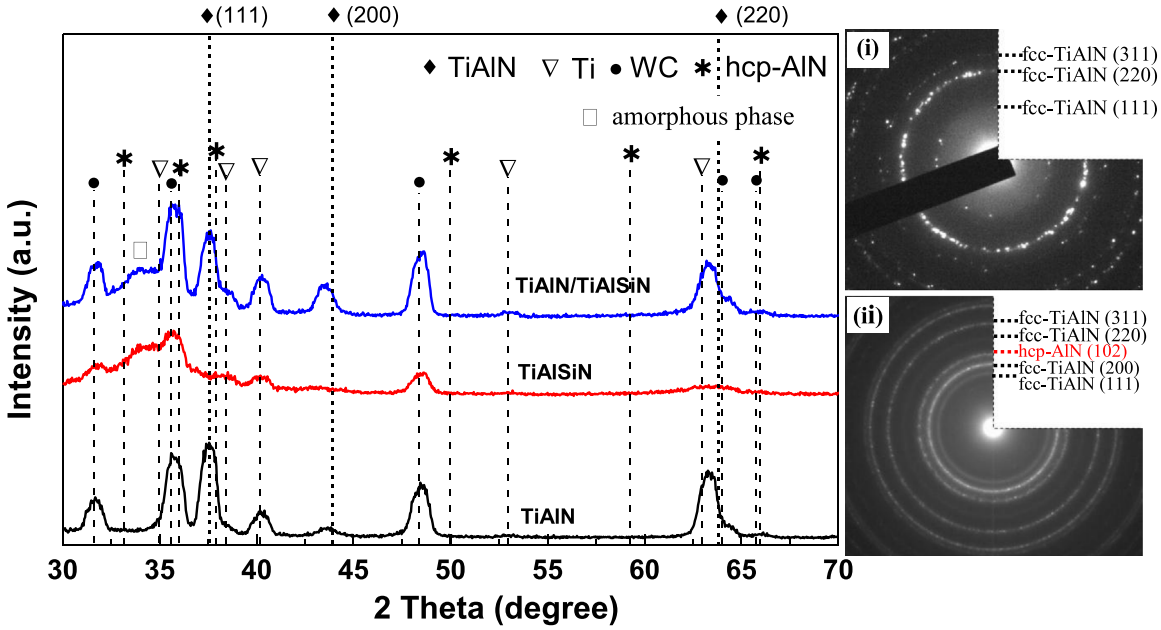

Fig. 3. XRD patterns of the TiAlN, TiAlSiN, and TiAlN/TiAlSiN coatings. The insets (i) and (ii) are the corresponding electron diffraction patterns of TiAlN and TiAlSiN, respectively.

to conduct an indentation experiments on above coatings with a load of 500 g. Fig. 9 gives a SEM image of indentation morphology. It can be observed that the TiAlN coating shows relatively small and light crack in the end of indentation in Fig. 9(a). This kind of crack morphology means a good toughness of TiAlN coating. However, the TiAlSiN coating shows relatively large and deep crack in Fig. 9(b). This means a bad toughness of TiAlSiN coating. And this can explain the premature spalling phenomena of TiAlSiN coating in scratch test. The TiAlN/TiAlSiN coating shows a better crack morphology than TiAlSiN coating, but worse than TiAlN coating.

3.3. Cutting experimental results

Cutting experiments were performed to investigate coated tool wear in turning titanium alloy under coolant condition. Tool wear was measured as the average flank wear land width (Vb) as a function of cutting length. The flank wear curves of the coated tools at different cutting speeds are depicted in Fig. 10. The coated tool is considered failure when the flank wear reaches to 0.3, as shown by dot lines in Fig. 10. It is observed that the cutting length of the TiAlSiN coated tool is the longest and is over 500 m at the cutting speed of 65 m/min.

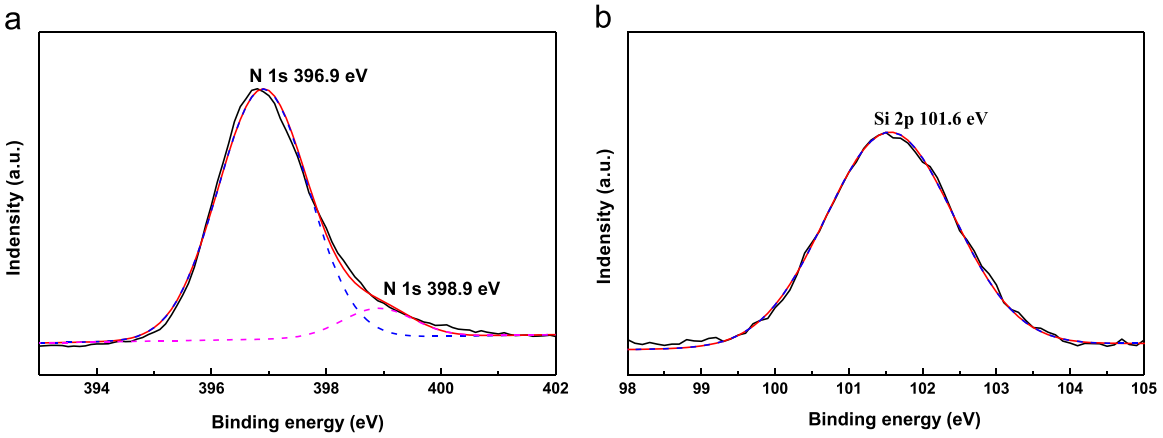

Fig. 4. XPS spectra of TiAlSiN coatings: (a) N 1s peaks; (b) Si 2p peaks.

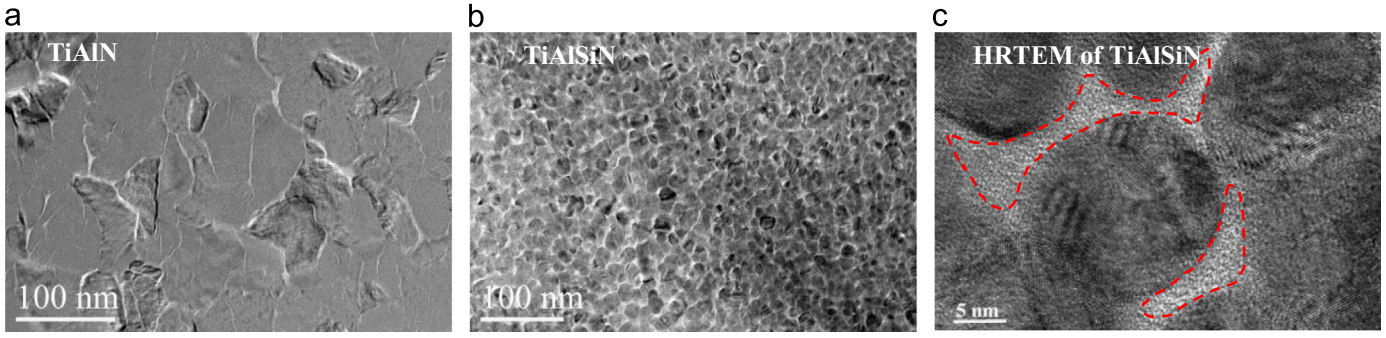

Fig. 5. TEM images of TiAlN and TiAlSiN coatings: (a) TiAlN coating; (b) TiAlSiN coating; and (c) HRTEM image of TiAlSiN coating.

The TiAlN/TiAlSiN composite coating has the shortest cutting length. The cutting length of the TiAlSiN is longer two times than that of the other two coated tools. When the cutting speed is increased to 100 m/min, similar case occurs. However, the cutting length was decreased to 120 m due to the worse working condition caused by the high cutting speed.

Fig. 11 shows the SEM morphology and the EDS results of TiAlN coated tools after turning titanium at the cutting speed of 65 m/min. It is found that the composition at point A is Ti, Al, V and C. The element V should come from workpiece materials, which means a built-up edge forms at point A. The built-up edge is related to the formation of intensive adhesive bonds (welds) at the coated tool/chip interface [2]. The built-up edge can lead to serious surface damage when it is torn off. Point B contains a relative high Co which comes from the cement carbide substrate. This means the coating at this location has been torn off and the cutting edge chipping occurs. Point C mainly shows the coating elements such as Ti Al and N. This means the coatings at this location are still existed.

In order to study the relationship of microstructure, properties and titanium cutting performance of these coatings, the surface and section morphology of these coated tools are observed as shown in Fig. 12. The results of all the coated tools indicate that a built-up edge and chipping of cutting edge occur. Thus, the major wear mechanism of these coated tools is adhesive wear and chipping under turning titanium alloy. With the cutting process continues, the built-up edge can tear off and take away partial coating and substrate material. The better

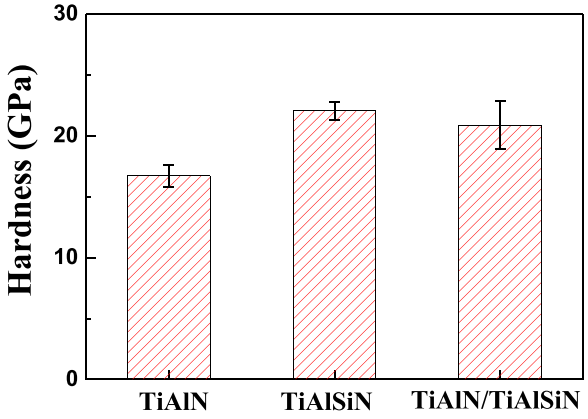

Fig. 6 Nanoindentation test results of different coatings: (a) TiAlN; (b) TiAlSiN; and (c) TiAlN/TiAlSiN.

machining performance of TiAlSiN coating in Fig. 10 can be attributed to its higher hardness and better oxidation resistance. The good oxidation resistance of TiAlSiN is mainly related to its fine nanocrystalline structure as shown in Fig. 2. However, the TiAlN and TiAlN/TiAlSiN coating contains a columnar structure, which can provide more high diffusion pathways for oxygen atoms [21,22]. This leads to a relatively bad oxidation resistance of TiAlN and TiAlN/TiAlSiN coating. In addition, the tool edge is cut at the location as shown by dashed box in Fig. 12. The section morphology of worn coated tool is observed. It is found that TiAlSiN coatings have dense and regular section morphology because of its fine nanocrystalline

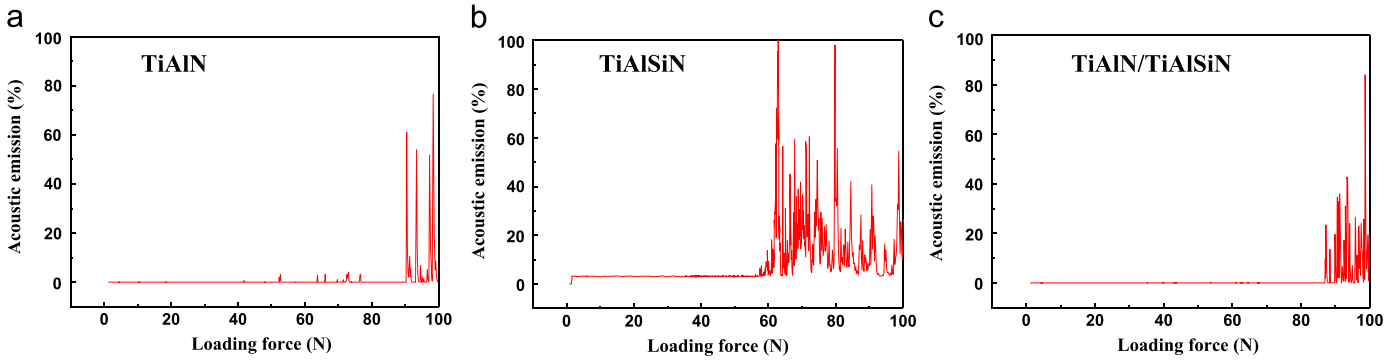

Fig. 7 Scratch test results of different coatings: (a) TiAlN; (b) TiAlSiN; and (c) TiAlN/TiAlSiN.

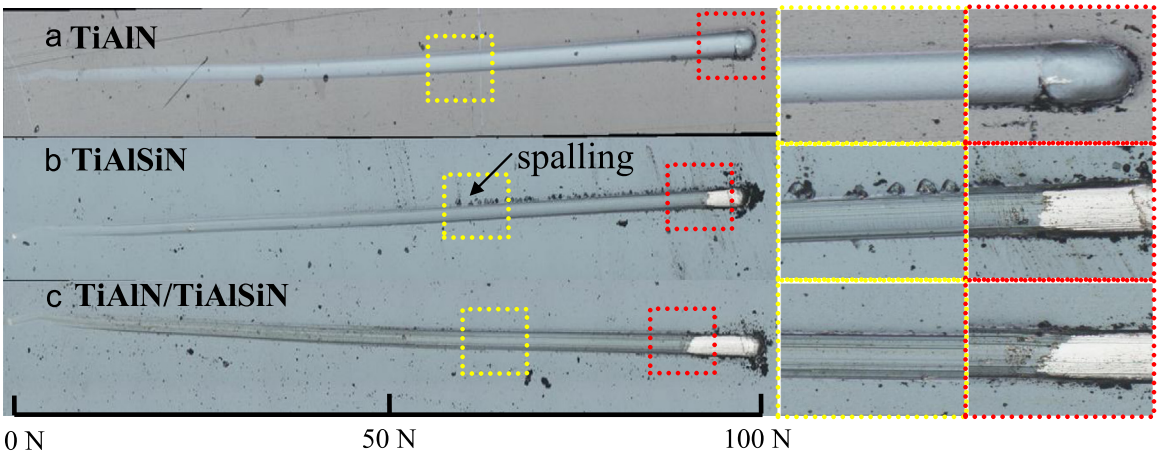

Fig. 8 Optical micrographs of scratch tracks of different coatings: (a) TiAlN; (b) TiAlSiN; and (c) TiAlN/TiAlSiN.

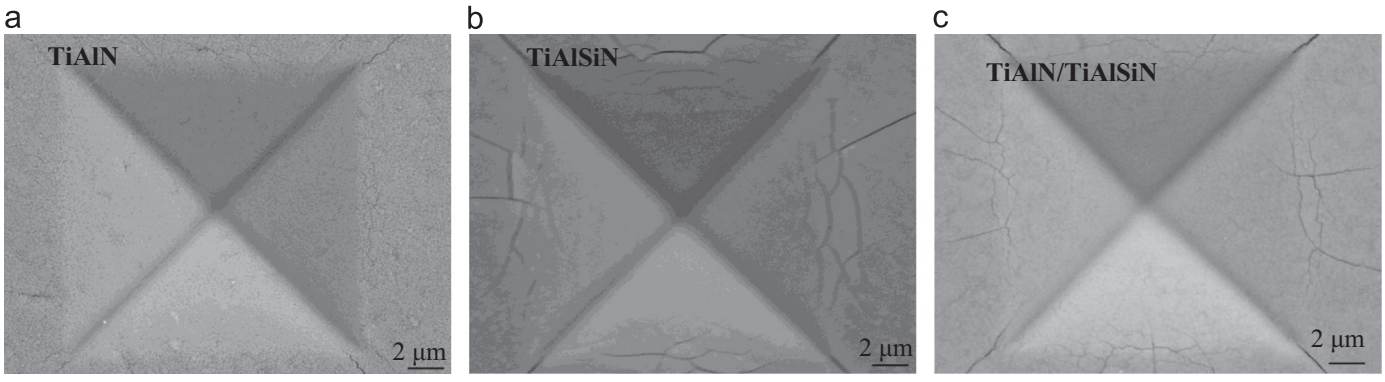

Fig. 9. SEM and schematic images of indentation of different coatings: (a) TiAlN; (b) TiAlSiN and (c) TiAlN/TiAlSiN.

structure. However, the TiAlN/TiAlSiN composite coating shows a severely broken and irregular morphology.

4. Conclusions

In this study, the relation of microstructure, mechanical properties and titanium cutting performance of the TiAlN, TiAlSiN and TiAlN/TiAlSiN coatings were studied. The main conclusions are listed as follows:

(1) The hardness of the TiAlN/TiAlSiN composite coating is 20.8 GPa which is higher than that of the TiAlN coating but is 5.6% lower than that of the TiAlSiN coating. And the TiAlN/TiAlSiN composite coating method can improve the premature spalling problem in TiAlSiN coating.

(2) When Si element is added to the coating, the morphology of coating changes from columnar to nanocrystal. The grain size was decreased at the same time. This nanocrystal structure suppressed the propagation of cracks in the coating and makes the crack morphology form a type of relatively regular and straight, which means good fracture toughness.

(3) The cutting performance of the TiAlSiN coating is the best at various cutting speeds. The maximum cutting length of the TiAlSiN coating exceeds 500 m at the speed of 65 m/

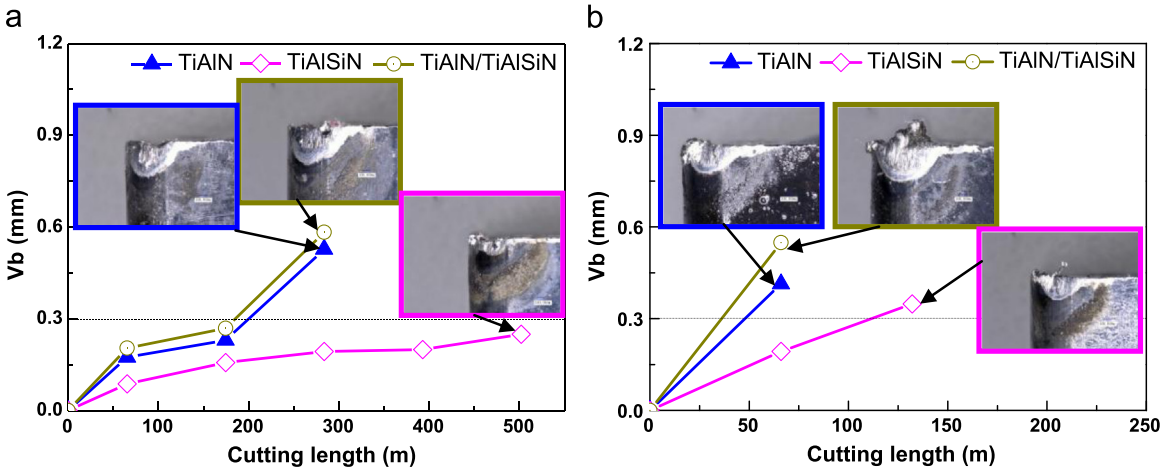

Fig. 10. Tool flank wear Vb curve versus cutting length at different cutting speeds: (a) 65 m/min and (b) 100 m/min.

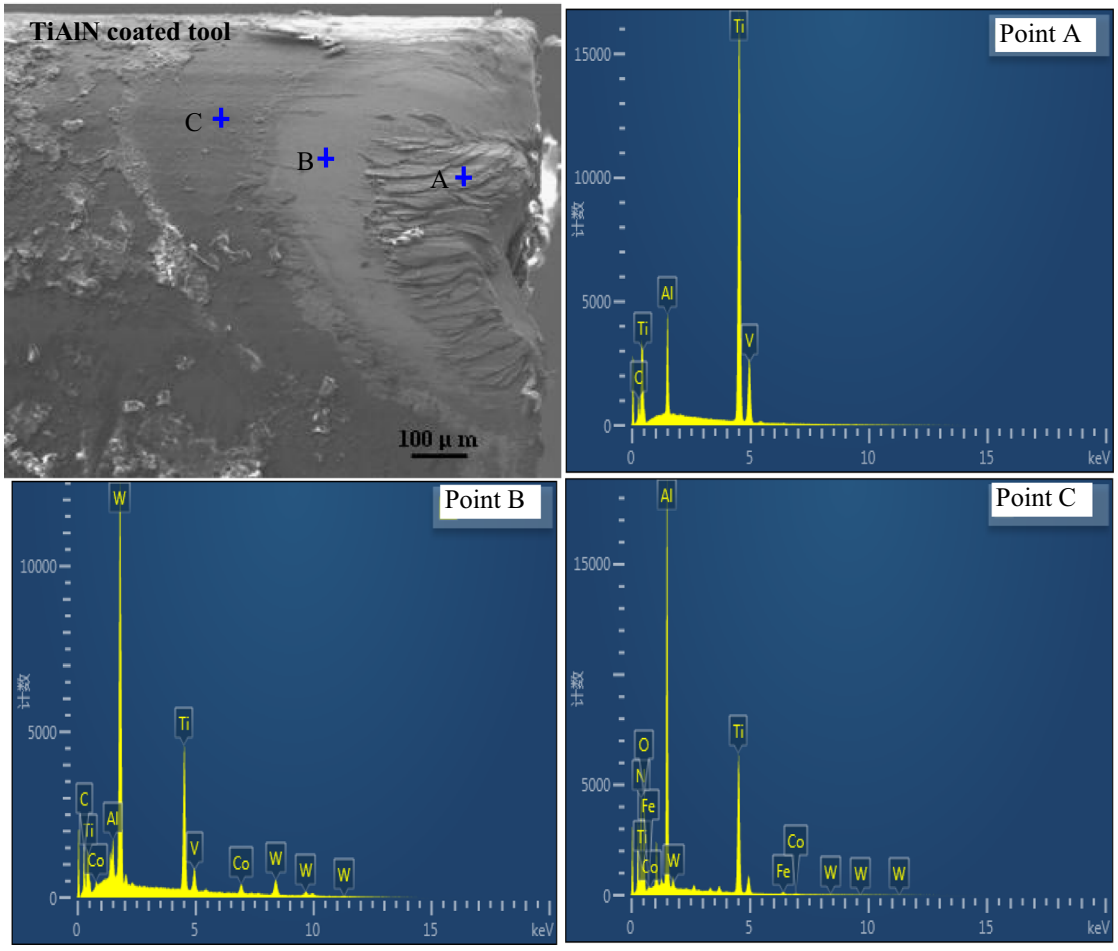

Fig. 11. SEM image and EDS results of the TiAlN coated tools after TC4 turned at 65 m/min.

min with coolant. The good cutting performance of the TiAlSiN coating is mainly related to its dense nanocrystal structure, high hardness and good oxidation resistance, which can lead to less area of built-up edge and chipping at the cutting edge.

(4) The major wear mechanism of these coated tools is adhesive wear and chipping in turning titanium. The TiAlSiN coating with dense structure, high hardness and good oxidation resistance is recommended to use in high speed turning titanium.

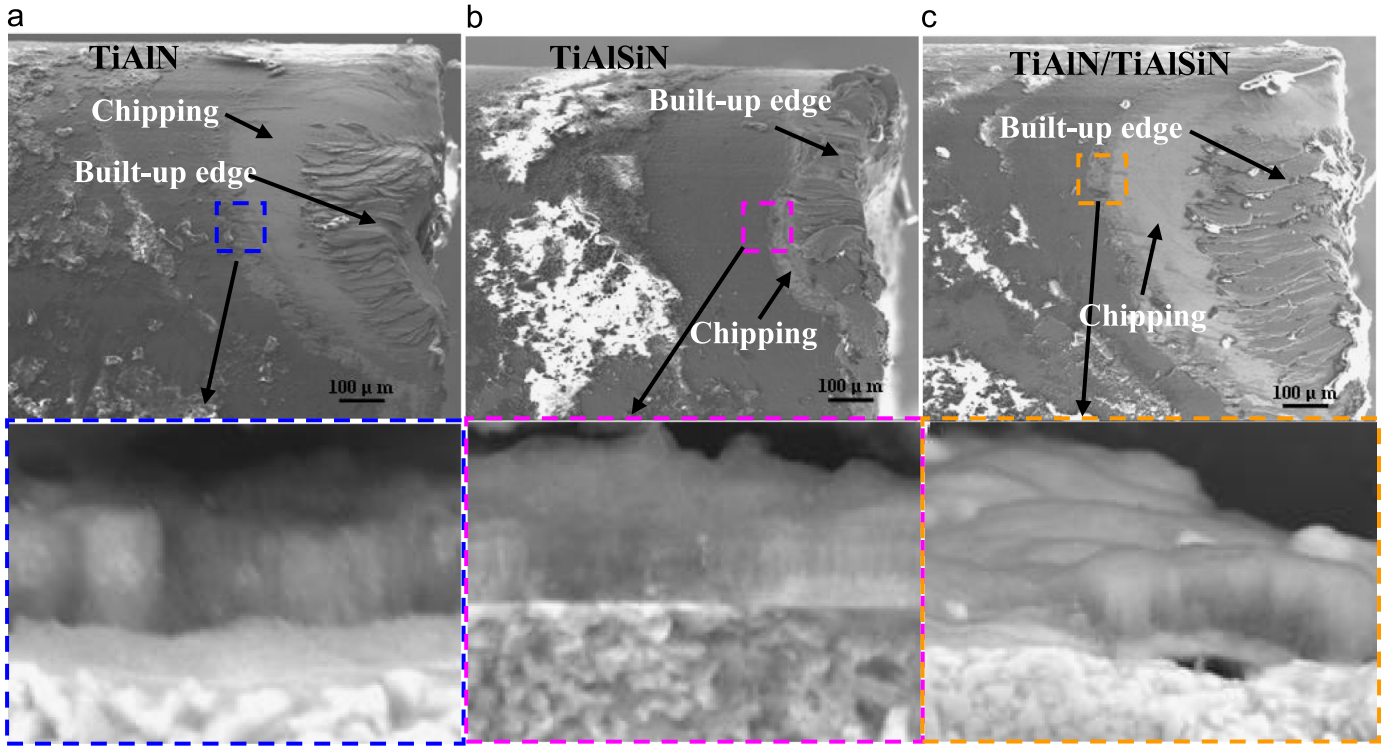

Fig. 12. SEM images of the coated tools after TC4 turned at 65 m/min: (a) TiAlN; (b) TiAlSiN; and (c) TiAlN/TiAlSiN.

Acknowledgements

The authors gratefully acknowledge the financial support of the National Science and Technology Major Project (2012ZX04003061).

References

[1] J. Davim, in: Machining of Titanium Alloy, Springer, 2014.
[2] A. Biksa, K. Yamamoto, G. Dosbaeva, S.C. Veldhuis, G.S. Fox-Rabinovich, A. Elfizy, T. Wagg, L.S. Shuster, Wear behavior of adaptive nano-multilayered AlTiN/MexN PVD coatings during machining of aerospace alloys, Tribol. Int. 43 (2010) 1491–1499.
[3] J.A. Ghani, C.H.C. Haron, S.H. Hamdan, A.Y.M. Said, S.H. Tomadi, Failure mode analysis of carbide cutting tools used for machining titanium alloy, Ceram. Int. 39 (2013) 4449–4456.
[4] J.H. Hsieh, C. Liang, C.H. Yu, W. Wu, Deposition and characterization of TiAlN and multi-layered TiN/TiAlN coatings using unbalanced magnetron sputtering, Surf. Coat. Technol. 108–109 (1998) 132–137.
[5] L. Chen, J. Paulitsch, Y. Du, P.H. Mayrhofer, Thermal stability and oxidation resistance of Ti–Al–N coatings, Surf. Coat. Technol. 206 (2012) 2954–2960.
[6] H.C. Barshilia, M. Ghosh, Shashidhara, R. Ramakrishna, K.S. Rajam, Deposition and characterization of TiAlSiN nanocomposite coatings prepared by reactive pulsed direct current unbalanced magnetron sputtering, Appl. Surf. Sci. 256 (2010) 6420–6426.
[7] T. Wang, G.J. Zhang, B.L. Jiang, Microstructure, mechanical and tribological properties of TiMoN/Si_3N_4 nano-multilayer films deposited by magnetron sputtering, Appl. Surf. Sci. 326 (2015) 162–167.
[8] T. Chen, Z.W. Xie, F. Gong, Z.Z. Luo, Z. Yang, Correlation between microstructure evolution and high temperature properties of TiAlSiN hard coatings with different Si and Al content, Appl. Surf. Sci. 314 (2014) 735–745.
[9] P.J. Arrazolaa, A. Garay, L.M. Iriarte, M. Armendia, S. Marya, F. L. Maître, Machinability of titanium alloys (Ti6Al4V and Ti555.3), J. Mater. Process. Technol. 209 (2009) 2223–2230.
[10] Y.H. Yoo, D.P. Le, J.G. Kim, S.K. Kim, P.V. Vinh, Corrosion behavior of TiN, TiAlN, TiAlSiN thin films deposited on tool steel in the 3.5 wt% NaCl solution, Thin Solid Films 516 (2008) 3544–3548.
[11] S. Veprek, H.D. Männling, M. Jilek, P. Holubar, Avoiding the high-temperature decomposition and softening of $(Al_{1-x}Ti_x)N$ coatings by the formation of stable superhard nc-$(Al_{1-x}Ti_x)N$/a-Si_3N_4 nanocomposite, Mater. Sci. Eng. A 366 (2004) 202–205.
[12] S.Q. Wang, L. Chen, B. Yang, K.K. Chang, Y. Du, J. Li, T. Gang, Effect of Si addition on microstructure and mechanical properties of Ti–Al–N coating, Int. J. Refract. Met. Hard Mater. 28 (2010) 593–596.
[13] D.H. Yu, C.Y. Wang, X.L. Cheng, F.L. Zhang, Microstructure and properties of TiAlSiN coatings prepared by hybrid PVD technology, Thin Solid Films 517 (2009) 4950–4955.
[14] L. Chen, S.Q. Wang, Y. Du, S.Z. Zhou, T. Gang, J.C. Fen, K.K. Chang, Y.W. Li, X. Xiong, , Machining performance of Ti–Al–Si–N coated inserts, Surf. Coat. Technol. 205 (2010) 582–586.
[15] S. Sharif, E.A. Rahim, Performance of coated- and uncoated-carbide tools when drilling titanium alloy–Ti–6Al4V, J. Mater. Process. Technol. 185 (2007) 72–76.
[16] Z.Q. Liu, Q.L. An, J.Y. Xu, M. Chen, S. Han, Wear performance of (nc-AlTiN)/(a-Si_3N_4) coating and (nc-AlCrN)/(a-Si_3N_4) coating in high-speed machining of titanium alloys under dry and minimum quantity lubrication (MQL) conditions, Wear 305 (2013) 249–259.
[17] A. Jawaid, S. Sharif, S. Koksal, Evaluation of wear mechanisms of coated carbide tools when face milling titanium alloy, J. Mater. Process. Technol. 99 (2000) 266–274.
[18] A. Miletic, P. Panjan, B. Škorić, M. Čekada, G. Dražič, J. Kovač, Microstructure and mechanical properties of nanostructured Ti–Al–Si–N coatings deposited by magnetron sputtering, Surf. Coat. Technol. 241 (2014) 105–111.
[19] S. Carvalho, L. Rebouta, E. Ribeiro, F. Vaz, Microstructure of (Ti,Si,Al) N nanocomposite coatings, Surf. Coat. Technol. 177–178 (2004) 369–375.

[20] N. Khanna, K. Sangwan, Interrupted machining analysis for Ti6Al4V and Ti5553 titanium alloys using physical vapor deposition (PVD)-coated carbide inserts, Proc. Inst. Mech. Eng. Part B: J. Eng. Manuf. 227 (2013) 465–470.

[21] C.M. Koller, R. Hollerweger, C. Sabitzer, R. Rachbauer, S. Kolozsvári, J. Paulitsch, P.H. Mayrhofer, Thermal stability and oxidation resistance of arc evaporated TiAlN, TaAlN, TiAlTaN, and TiAlN/TaAlN coatings, Surf. Coat. Technol. 259 (2014) 599–607.

[22] R. Hollerweger, H. Riedl, J. Paulitsch, M. Arndt, R. Rachbauer, P. Polcik, et al., Origin of High temperature oxidation resistance of Ti–Al–Ta–N coatings, Surf. Coat. Technol. 257 (2014) 78–86.